CCF Transactions on Pervasive Computing and Interaction
https://doi.org/10.1007/s42486-021-00080-4

REGULAR PAPER

Feasibility study of practical vital sign detection using millimeter-wave radios

Weicheng Wang[1] · Zhenhua Jia[2] · Chenren Xu[1] · Guojie Luo[1] · Daqing Zhang[1] · Ning An[3] · Yanyong Zhang[4]

Received: 3 July 2021 / Accepted: 8 October 2021

Abstract

The importance of vital sign detection is self-evident in the mobile health domain. Recent work has shown that one can use RF or WiFi signals for respiration and heartbeat detection in a non-contact manner and thus improve its usability compared to the wearable-based solution. However, the existing approaches either require an ultra-wideband radio which is not commercially available or do not perform well in practical working environments. The millimeter-wave (mmWave) radio is a promising solution for fine-grained heartbeat and respiration sensing applications because of its directionality and sensitivity. However, we find traditional mmWave algorithms suffer from background noise in practical scenes. In this article, we address this issue by designing a robust algorithm for heart rate detection based on time-domain and frequency-domain information. We implement a phase-modulated system on the software-defined radio platform and evaluate the algorithm performance. Also, we evaluate the impact of several practical factors, such as detecting distance, aiming point, depression angle, human orientation and beam width on the proposed heart rate algorithm. Finally, we explore the feasibility of mmWave on vital sign detection with strong background interference and in scenes of real life where the antennas are hanging on the ceiling. The results show that the mean estimation error of respiration and heartbeats are 0.487 Bpm and 2.386 bpm.

Keywords Wireless sensing · Vital signs · Millimeter-wave · Mobile health

1 Introduction

Respiratory rate (RR) and heart rate (HR) are two of the most important vital signs that indicate the severity of a patient's condition. Traditional approaches use dedicated sensors to measure vital signs in clinical research. For example, Holter monitors are used for ambulatory monitoring during the recovery period after cardiac surgeries (Zimetbaum and Josephson 1999), and conventional non-invasive monitoring of respiratory rate is performed by impedance pneumography (Grenvik et al. 1972) and inductive plethysmography. These systems meet the clinical requirement in terms of high accuracy, but they are invasive and cumbersome which obstructs them from daily use.

As the market of mobile health (mHealth) technology is rapidly evolving, researchers begin to pay attention to new mobile technologies potentially available for health care systems. Quite a few research has shown the great potential and benefits of introducing vital sign detection into people's daily life, such as physical health tracking, sleep quality monitoring (Bianchi et al. 2010), mental stress assessment (Sun et al. 2010) and so on. However, towards building a

✉ Chenren Xu
chenren.xu@gmail.com
http://ceca.pku.edu.cn/chenren

Weicheng Wang
wangweicheng@pku.edu.cn

Zhenhua Jia
zjia@nvidia.com

Guojie Luo
gluo@pku.edu.cn

Daqing Zhang
dqzhang@sei.pku.edu.cn

Ning An
ning.g.an@acm.org

Yanyong Zhang
yanyongz@ustc.edu.cn

1 Peking University, Beijing, China

2 NVIDIA, New Jersey, United States

3 Hefei University of Technology, Anhui, China

4 University of Science and Technology of China, Anhui, China

Published online: 15 November 2021

practical system for daily vital sign monitoring, we face different challenges compare to the traditional approach: the system should be easy to use, non-invasive, and should support mobility. Recently advances in smartphones and wearable sensors have enabled daily vital sign monitoring, such as smart bracelets for monitoring heart rate and chest belts for monitoring respiratory rate. Apparently, these wearable devices are inconvenient for users who have sensitive or fragile skins, for example, users like children, elders, patients critically burned, etc.

As such, a good non-contact vital sign monitoring system is in desire. Previous work has shown it is possible to achieve non-contact vital sign detection based on RF signal (Adib et al. 2015). The authors use a customized FMCW (Frequency Modulated Carrier Waves) radio, sweeping from 5.46 to 7.25 GHz, to separate vital signs from different users in a multi-user scene. Meanwhile, considering the cost of the radio platform, many researchers take advantage of the off-the-shelf WiFi-enabled devices to detect human's vital signs (Ravichandran et al. 2015; Abdelnasser et al. 2015; Wang et al. 2016; Liu et al. 2015; Wang et al. 2017a, b; Zeng et al. 2018; Zeng et al. 2019). However, WiFi signal has some inherent limitations. When detecting multiple humans at the same time, the received signal can be reflected from multiple people because of the commonly used omni-directional antenna. To estimate respiratory rate of multiple persons, complex signal processing methods, such as tensor decomposition (Wang et al. 2017b) and root-MUSIC (Wang et al. 2017a), should be employed to handle the reflected signal. This makes it difficult to estimate heart rate of multiple persons from the tiny motion of heartbeats according to the reflected signal.

As one of the critical technologies of the upcoming fifth-generation wireless systems, millimeter-wave (mmWave) technology provides a unique and promising solution to overcome many sensing challenges in vital sign detection. The biggest advantages are its significantly larger bandwidth and higher spatial resolution. Combined with the availability of a phased array antenna, mmWave can use a narrow beam to detect a single user at one time, switch the beam direction in nanoseconds and eventually monitor the vital signs of multiple users in parallel. MmVital (Yang et al. 2016) uses the received signal strength (RSS) of the 60 GHz signal to locate human body in a room. What's more, they study the vital sign detection of multiple users concurrently and evaluate their system in multi-user scenes. However, RSS is insensitive to the minute chest movements caused by respiration and especially the more minute heartbeat according to our feasibility study in Sect. 5.3. Therefore, the experimental setup of their work is not practical enough, and for HR detection they assume that the antennas are on the same height as user's chest and the HR detecting distance is limited to 3 meters.

In this paper, we propose a robust vital sign detection system, called *MiVital*, using millimeter-wave (mmWave) radios within a larger distance range in more practical environments. *MiVital* is a phase modulated system on the software-defined radio platform for monitoring respiratory rate and heart rate. The advantages of using mmWave with phase modulation are its higher spatial resolution compared to WiFi signal because of its short wavelength and its ability to separate multiple users with the availability of a phased array antenna.

Our system first measures the phase delay of a reflected mmWave signal caused by the slight distance changes along the signal path. Such small changes are introduced by the chest moving back and forth during the respiration and heartbeat activities. The estimation of RR is easy because the body displacement caused by respiratory holds the dominant position in the change of phase delay. To further estimate user's HR, there are two traditional methods termed by us as the time-domain information based HR detection (TiHR) and the frequency-domain information based HR detection (FiHR). Both of them have their advantages and perform well when the user is close to the antennas in the previous simple scene. However, when the detecting distance gets larger and antennas hang on the ceiling, the accuracy rates of both the existing algorithms will decrease seriously. FiHR suffers from its global instability that the signal in the frequency domain may have a misleading peak, while TiHR suffers from its local sensitivity that the signal in the time domain may be disturbed by breathing harmonics and user's unconscious jitters. To improve the robustness of HR detection, we develop a *Time-domain and Frequency-domain Information Based HR Detection* algorithm combining both the advantages of TiHR and FiHR. Specifically, we take advantage of TiHR's global stability by calculating a reference HR value according to the acceleration of phase delay in the time domain, and then use the reference value to avoid selecting the wrong peak in the frequency domain. After selecting a reliable frequency peak, we apply the HR estimation methods in FiHR to make use of its local insensitivity.

Besides, we further study the accuracy of heart rate estimation versus the environmental factors such as detecting distance, aiming position, depression angle, human orientation and beam width. Finally, we evaluate the performance of our system with strong background interference and in practical scenes of imitating a ceiling-mounted access point. The results show that the mean estimation errors of RR and HR are 0.487 Bpm and 2.386 bpm in the working range, which is comparable with the state-of-the-art results, and our system can work at a larger range up to 7 meters with the 34 dBi antennas.

In summary, our contributions are:

1. We design a time-domain and frequency-domain information based heart rate estimation algorithm to improve its robustness to background noise in comparison with two existing algorithms using the mmWave radio.
2. We implement and evaluate our designed vital sign detection system on the 60 GHz software-defined radio platform, and our experimental results show we can achieve 0.487 Bpm and 2.386 bpm estimation error of respiratory rate and heart rate, respectively.
3. We study the impact of detecting distance, aiming position, depression angle, human orientation and beam width on the performance of our system based on the estimation results and further evaluate vital sign detection with strong background interference and in the daily working environment through an access point mounted on the ceiling or on the wall.

2 Related work

2.1 Contact-based vital sign detection

Quite a few research has been done using the contact-based approach. We categorize these systems into several groups based on the sensor modality: systems using force sensors (Bruser et al. 2011; Chung et al. 2007), velocity sensors (Jia et al. 2016, 2017), accelerometers (Bonde et al. 2018; Phan et al. 2008), pressure sensors (Rosales et al. 2012; Anttonen et al. 2005; Kortelainen et al. 2012),capacitive proximity sensors (Griffiths et al. 2014), optical sensors (Šprager and Zazula 2013), etc. Even though many systems have been proposed, few are easy to use, non-invasive, and location-independent all at the same time. For example, some systems detect the heartbeats but require some specially designed hardware sandwiched between the bed frame and mattress (Rosales et al. 2012); some systems require a user to lean his/her back against the backrest of a chair in order to get accurate respiration detection (Griffiths et al. 2014); some systems only work for some fixed locations (Bruser et al. 2011; Kortelainen et al. 2012); some system can only detect one type of vital signs (either respiratory rate or heart rate) but not both (Jia et al. 2016; Bonde et al. 2018); most of the systems require direct contact with either the sensor or some kind of medium (chair, bed, etc.) which limit users' mobility; also, most of the systems fail to handle multiple users.

2.2 Non-contact vital sign detection

Adib et al. (2015) used FMCW radio sweeping from 5.46 GHz to 7.25 GHz to separate multiple quasi-static users into different buckets. But their system uses customized hardware and is not suitable for promotion to daily usage. Recently, researchers are interested in using WiFi signal of 2.4/5 GHz (Ravichandran et al. 2015; Abdelnasser et al. 2015; Wang et al. 2016; Liu et al. 2015; Zeng et al. 2018; Wang et al. 2017a, b; Zeng et al. 2019). Authors in Ravichandran et al. (2015) and Abdelnasser et al. (2015) use the RSS of WiFi signal to detect vital signs and can only estimate the respiratory rate, while authors in Liu et al. (2015) use channel state information (CSI) of WiFi to estimate the respiratory rate and heart rate at the same time. And authors in Wang et al. (2016), Zeng et al. (2018) introduce the Fresnel zone model for respiratory rate detection using WiFi. But with the inherent limitation of WiFi signal, it's difficult for their work to distinguish users with similar vital signs. The work of Wang et al. (2017a, 2017b) exploits WiFi CSI phase difference between two receiver antennas to extract respiration rate and heart rate. Apart from the RF signal, researchers also succeed in measuring heart rate based on videos (Li et al. 2014). They take advantage of cameras to capture the skin color change caused by the cardiac pulse. However, the detection region needs to be illuminated throughout the entire monitoring duration, which is obtrusive. Further, the vital sign is so useful that many researchers succeed in accomplishing some interesting work. Authors in Zhao et al. (2016) use features of the heartbeat to recognize user's emotion. And authors in Lin et al. (2017) develop an authentication system based on the features of the heartbeat. The usage of motors also allows researchers to monitor sleepers with body turns and estimate their breathing volume (Nguyen et al. 2016).

2.3 MmWave sensing and networking

The mmWave shows great potential in non-contact sensing because of its short wavelength. Using mmWave radios, researchers have achieved sub-centimeter scale object localization/tracking (Wei and Zhang 2015), temperature sensing using low-cost cholesteryl tags by thermal scattering effect (Chen et al. 2020), material recognition based on the reflection signals in both static and mobile cases (Chenshu et al. 2020) and non-intrusive micrometer-level vibration measurement (Jiang et al. 2020). Using commodity 60 GHz phased array antennas, mmWave technologies are able to sense more complex motion. Authors in Wu et al. (2020) achieve high spatial resolution multi-person localization/tracking passively and authors in Santhalingam et al. (2020) achieve American sign language gesture recognition with 87% average accuracy. In the aspect of vital signs monitoring, the authors in Jason Kao and Lin (2013) and Chuang et al. (2012) have discussed vital sign detection using 60 GHz mmWave. But their work focuses on the theoretical foundation and assumes there is only one user in the close distance. In recent, authors in Yang et al. (2016) focused on

solving the practical challenges of finding the human location in a room and detecting vital signs of multiple people concurrently. To verify the robustness of their work to distance, they study the impact of distance on RR accuracy. But they avoid discussing the impact of distance on HR accuracy and only estimate HR within 3 meters.

MmWave technologies also show their great development potential in wireless communication because of mmWave's large spectrum resource. MmWave can further improve its spectral efficiency through the first mmWave massive MIMO software radio (Zhao et al. 2020).

3 Understanding vital sign detection

In this section, we first discuss the theoretical foundation of distance detection and further chest movement detection based on mmWave. Then, we analyze the typical features of respiratory and heartbeats. Finally, we introduce the existing algorithms for respiratory rate (RR) and heart rate (HR) detection.

3.1 Principle of RF distance detection

Consider the simplest scene that we have a pair of transmitter and receiver equipped with directional antennas and point them to the target. To measure the length change along the signal path, our system continuously emits a packet of the tone signal with a fixed interval of less than one millisecond. At the same time, it receives the reflected signal and analyzes the phase delay. If there is only one signal path reflected, the phase delay of RF is proportional to the RF signal path length (Tse and Pramod 2005). Although our system is not able to obtain the absolute values of these two variables, we can still detect the variation of them according to the equation: $\Delta\phi(t_n) = -\frac{2\pi f \Delta D(t_n)}{c}$. Here $\Delta\phi(t_n)$ is the first order difference of received signals' phase delay $\phi(t_n)$, f is the frequency of RF signal and $\Delta D(t_n)$ is the first order difference of the signal path length $D(t_n)$.

3.2 Human body movement detection

To analyze the reflections from a more practical human body, we first need to properly model it. Although a human body could be considered as a combination of many layers in sequence: clothing, skin, subcutaneous adipose tissue (SAT), muscle and so on, more than 90% of the transmitted power is absorbed in the epidermis and dermis layer as mentioned in Wu et al. (2015). Besides, most power of mmWave signal can be propagated through clothing. As such, one layer of skin is sufficient for a reliable electromagnetic evaluation in our study.

Next, the layer of skin is not a flat "mirror" but a rough surface. When the beams of antennas are focused on the human body, the reflection region is the range of the human body illuminated by the transmitter. According to Li and Lin (2008), respiration and heartbeats lead to different movements and these movements may vary across different parts of the human body. Thus, the mmWave signal path reflected from these parts of the human body leads to different phase delays. And the received signal we obtain is the sum of reflected signals in the beam range of receiver's antenna. Thus, the $\Delta D(t_n)$ calculated from the received signal does not represent the length change of a single reflected signal path. Rather, it is the result of the length changes of all the reflected paths.

Then the question is how to get RR and HR from the measured $\Delta D(t_n)$. The idea is as follows: *although the amplitude attenuation and the phase delay of each signal path are unknown, the features of each path have the quasi-synchronous changes with human body's periodic motion caused by respiration and heartbeats.* Therefore, the sum of reflected signals also has synchronous changes, from which we can detect human body's periodic motion without accurately measuring the detailed displacement of the human body.

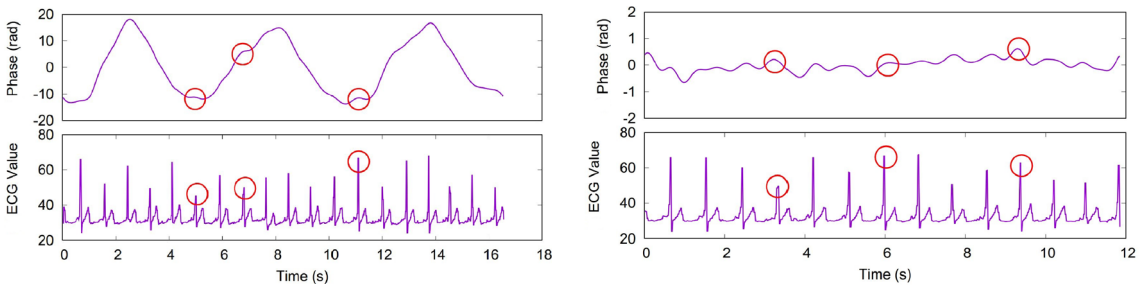

(a) Respiratory together with heartbeat

(b) Heartbeat without respiratory

Fig. 1 Phase change detected by our system and ground truth of ECG output for two scenes with/without respiratory. The large variations in **a** represent respiration and the small variations in red circles represent heartbeat

3.3 Features of respiratory and heartbeats

Before going into the details about measuring HR and RR, we first explain how the phase varies with vital signs. According to work in Adib et al. (2015), the change of phase delay is mainly caused by the expansion and contraction of user's chest, which is synchronous with user's respiration. In this paper, we consider that the typical respiratory rate for an adult at rest is between 8 and 16 breaths per minute (Bpm), as mentioned in U.S. National Library of Medicine (2018). Figure 1a shows the phase delay over time, measured with our 60 GHz system. The fluctuation of the phase delay is caused by respiratory and heartbeats. The peaks and valleys correspond to exhale and inhale motions of the user, and the small variations in the red circles represent user's heartbeats. To verify the heartbeats, we can compare the red circles in Fig. 1a with those of ECG output as ground truth in Fig. 1a.

Heartbeats cause slight skin movements of user's chest, and a normal resting heart rate for adults ranges from 60 to 100 beats per minute (bpm) as mentioned in Mayo Clinic (2018). The physiological phenomenon of ballistocardiography (BCG) makes the heart rate easier to detect, which refers to movements of the body synchronous with the heartbeats due to ventricular pump activity (Eduardo et al. 2010). We show an example experiment measured with our system in Fig. 1b. Here, we ask the user to hold his breath deliberately in order to clearly show the phase change caused by heartbeats. We observe that the phase peaks in Fig. 1b are synchronous with the peaks of ECG output in Fig. 1b and the red circles are three examples.

3.4 Existing algorithms for RR and HR measurement

Since the quasi-static user may consciously move his limb or change his posture sometimes, previous work (Adib et al. 2015) preprocess the original phase/RSS data by discarding the intervals of time when the data change rapidly. Then in order to measure the respiratory rate, the simplest method is to count the number of phase peaks after applying a peak detection algorithm. However, if the user has unconscious jitters or sudden changes from background sometimes, this method is unable to distinguish the peaks caused by respiration from noise. Therefore, the authors in Adib et al. (2015) and Yang et al. (2016) use frequency-domain dominating methods. They collect phase or RSS sequence for the time of a fixed window and use Fast Fourier Transformation (FFT) to change the sequence from the time domain to the frequency domain. Then they select the highest peak, apply a custom filter according to the peak and use linear fitting or peak detection to get a more accurate measurement of respiratory rate.

As for heart rate measurement, more complex algorithms are leveraged because of the minute chest movement caused by heartbeats and interference from breathing harmonics. We classify the HR detection methods used in Adib et al. (2015), Yang et al. (2016), Zhao et al. (2016) into two types as follows.

Frequency-domain Information based HR Detection (FiHR). The authors in Adib et al. (2015) and Yang et al. (2016) use the similar idea in RR detection to measure HR. They focus on the peaks in the frequency of about [40-200] bpm to separate heartbeats from respiration's first harmonic. To get rid of respiration's higher harmonics, FiHR will remove the peaks that correspond to breathing harmonic and select the highest peak from the remaining ones. The remaining steps are the same with RR measurement to get a more accurate measurement of heart rate according to the selected peak.

Time-domain Information based HR Detection (TiHR). According to work in Zhao et al. (2016), breathing is usually slow and steady while a heartbeat involves rapid contraction of the muscles. Therefore, the acceleration of breathing is smaller than that of heartbeats. In order to segment the acceleration signal into individual heartbeats, they formulate an optimization problem to find the periodic pattern corresponding to each heartbeat cycle. After that, they can easily measure the heart rate by counting the number of individual heartbeats.

Without eliminating the interference of breathing harmonic, the HR estimation performance of TiHR is not as good as FiHR. On the other hand, the frequency resolution of FiHR is the reciprocal of FFT window length which is a tradeoff between accurate vital sign estimating and quick reaction to vital sign change. However, TiHR can react to an increase or decrease in HR immediately. Another advantage of TiHR over FiHR is the ability to estimate the inter-beat-interval (IBI) for other purposes such as emotion recognition (Zhao et al. 2016) since TiHR can separate each heartbeat in the time domain.

4 Hart rate detection in practical scenes

4.1 Simple scenes and practical scenes for HR detection

Based on the technique of mmwave, mmVital (Yang et al. 2016) uses the same 60 GHz frontends as ours. The most commonly evaluated scenario for HR detection in mmVital is a simple scene where the quasi-static user stands or sits in front of the antennas with the chest movements caused by respiratory and heartbeats. Specifically, the user can move his limb or change his sitting posture sometimes. The antennas are at the same height as user's chest, and the

HR detecting distance is limited to 3 meters. In this scene, the variety of phase delay or RSS mainly consists of respiratory, heartbeats and tiny background changes. Then the major noise is the interference from breathing harmonics. Besides, there are also unconscious jitters of user as well as tiny changes from background and phase noise.

In more practical scenes discussed in this paper, the transmitter and the receiver are not close to the user but hanging on the ceiling or on the wall. And the detection range is extended to the whole room. When the detecting distance gets longer, the illuminated range will get larger and introduce more noise from the background. Then the impact of chest movement on the received signal will also get smaller. In this practical case, the tiny change from background and phase noise of hardware will play a more important role. We conclude all the noise sources for two scenes in Table 1 and now we'll analyze the impact of these noise sources on HR detection of FiHR and TiHR in practical scenes.

To deal with noise source of type 1, the original phase/RSS data are preprocessed by discarding the intervals of time when the data change rapidly. As for noise sources of type 2 and 3, they will impact the time domain information obviously. And the HR measurement will not be accurate enough when just considering the local fluctuation of phase acceleration. We term this property as the local sensitivity of TiHR. However, by focusing on the frequency domain and remove breathing harmonic peaks, FiHR can mitigate these two noise sources and magnify the periodicity effect of heartbeats, which is termed as the local insensitivity of FiHR. A strong noise source of type 4 is the key feature of the practical scene. Once the periodicity effect of minute heartbeats is as weak as being overwhelmed by the background and phase noise, a "misleading peak" for HR measurement in the frequency domain will appear. Figure 2 shows an example of a misleading peak. Here the true HR peak is 1.05 Hz according to the ground truth of ECG output, but the highest peak in the range of [0.7 Hz, 2 Hz] is 0.79 Hz. This happens because the beam width of 20^o introduces strong reflected signals from the background within the detection distance of 3 meters and the effect of heartbeats is quite weak. In this case, FiHR will lead to a significant

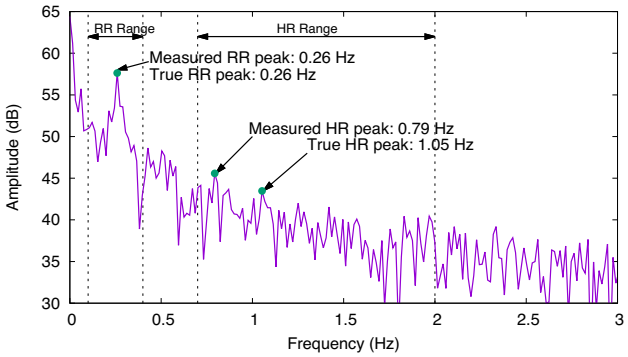

Fig. 2 An example of a misleading HR peak in FiHR. The measured RR peak is exactly the true RR peak because of the obvious periodicity of respiratory, while the measured HR peak is a misleading peak when the periodicity effect of the heartbeats is overwhelmed by environmental noise

measurement error of up to tens of percent, and we term this property as the global instability of FiHR. On the other hand, TiHR preserves the complete frequency information of heartbeats by applying acceleration rather than focusing on the peak of heartbeats' first harmonic. Therefore, noise source of type 4 has a limited influence on TiHR and we term this property as the global stability of TiHR. From the above analysis, we can find that both the global instability of FiHR, and the local sensitivity of TiHR decrease the accuracy of HR estimation. Therefore, we explore how to leverage both the global stability of TiHR and the local insensitivity of FiHR and propose our algorithm in the next section.

4.2 Time-domain and frequency-domain information based HR detection

To improve the robustness of the heart rate detection algorithm, we employ a *Time-domain and Frequency-domain Information based HR Detection* (TFiHR) algorithm which combines the ideas of FiHR and TiHR. The specific design idea of TFiHR is as follows. First, TFiHR discards the intervals of time when the data change rapidly. Then If the gap between the highest peak with the other peaks in HR

Table 1 Four types of noise sources and their impacts in previous simple scene and current practical scene

Type	Noise sources	Scene in mmVital (Yang et al. 2016)	Practical Scene in this paper
1	Conscious limb move or posture change of user	+	+
2	Unconscious jitters of user	+	+
3	Interference from breathing harmonics	+	+
4	Tiny changes from background and phase noise	–	+

"–" represents the impact of noise source is small while "+" represents the impact is large

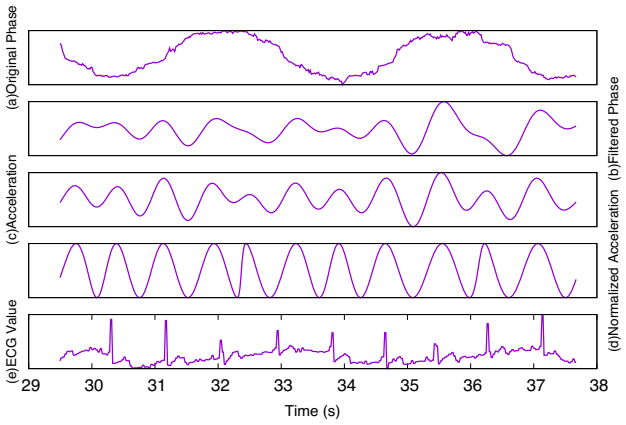

Fig. 3 The effect of acceleration in TFiHR. **a** The original phase signal; **b** the filtered phase with cutoff frequencies between [0.5–5] Hz; **c** the acceleration of the filtered phase which has more obvious periodicity; **d** the normalized acceleration; **e** the ground truth of ECG output. The peaks of the normalized acceleration are basically synchronous with those of ECG output

Fig. 3b. Then according to work in Zhao et al. (2016), we use the second order differentiator to express the acceleration of the signal ($\phi''(t_n)$). In Fig. 3c, we can find that the periodicity of the acceleration signal is more obvious than that of filtered phase signal in Fig. 3b. Before separating the acceleration by peaks, we will normalize the acceleration signal to reduce the influence of amplitude fluctuations. Specifically, we first generate the analytic version of signal by taking it and then adding its Hilbert Transform (Høst-Madsen et al. 2008) as $\phi''_a(t_n) = \phi''(t_n) + j\mathscr{H}(\phi''(t_n))$, where $\mathscr{H}(\cdot)$ is the Hilbert Transform. As we only care about the periodicity of each heartbeat cycle for HR estimation, we normalize the acceleration signal by dividing the complex magnitude to enlarge the heartbeat periodicity and get $\phi''_N(t_n) = \phi''(t_n)/|\phi''_a(t_n)|$ as shown in Fig. 3d. Then after removing the peaks that correspond to breathing harmonic, we use the reference value to find the peak in the frequency domain with maximum probability.

Algorithm 1 Time-domain and Frequency-domain Information based HR Detection (TFiHR)

Input: The set of phase delays $\phi(t_n)$ and sample rate f_s;
Output: Heart rate measurement f_{HR};
Discard the intervals of time when the data change rapidly
$\Phi(\omega_n) \leftarrow FFT(\phi(t_n))$
Find the peaks of $\Phi(\omega_n)$ between [0.7-2] Hz, and label the highest as $\Phi_{max} = \Phi(f_1)$
if $\Phi(f_1)$ is much higher than the other peaks
  $ref \leftarrow f_1$
else
  Filter $\phi(t_n)$ between [0.5-5] Hz and calculate its acceleration as $\phi''(t_n)$
  $\phi''_a(t_n) \leftarrow \phi''(t_n) + j\mathscr{H}(\phi''(t_n))$
  $\phi''_N(t_n) \leftarrow \phi''(t_n)/|\phi''_a(t_n)|$
  Abandon cycles with distortion from $\phi''_N(t_n)$ and get the average interval length l, $ref \leftarrow f_s/l$
end if
Remove the peaks between $[ref - 0.1Hz, ref + 0.1Hz]$ that correspond to breathing harmonic
From the remaining peaks between $[ref - 0.1Hz, ref + 0.1Hz]$, label the highest one as $\Phi(f_2)$
Create a custom narrow band-pass filter to extract signal from the neighborhood of f_2 and get $\Phi_{HR}(\omega_n)$
$\phi_{HR}(t_n) \leftarrow IFFT(\Phi_{HR}(\omega_n))$
Separate periodic segment of $\phi_{HR}(t_n)$ and get the average interval length l_{HR}, $f_{HR} \leftarrow f_s/l_{HR}$
return f_{HR};

frequency range is larger than a threshold, we believe that the highest peak is apparent enough and it represents the periodicity of the heartbeats. Then we'll just use the frequency of this peak as a heart rate reference value *ref*. Otherwise, we will employ part of methods in TiHR to help find the heart rate reference value.

As can be seen from Fig. 3a, the heartbeat pattern in the original phase ($\phi(t_n)$) is covered by respiration pattern and noise. Thus we first apply a high-order bandpass filter with cutoff frequencies of 0.5Hz and 5Hz and get the signal in

Overall, it's easy to find a strong relationship between the ground truth of ECG output value and normalized acceleration. However, the peaks of normalized acceleration are not aligned with those of ECG output. What's worse, we can find the normalized acceleration (shown in Fig. 3d) during the 32nd to 34th second has one more peak compared to the ECG output (shown in Fig. 3e). Therefore, we need to abandon signal with distortion to reduce the effect of noise. We first divide the normalized acceleration into cycles according to the peaks. Then, we scan through the

cycles and identify any cycle with abnormal intervals compared to its neighbors. Obviously, the interval of the cycle between about 32 and 34 s is distorted seriously compared to its adjacent neighbors and should be abandoned. Next, we use the remaining periodic cycles to calculate the reference heart rate *ref*. The reference rate is further used for helping find the most likely peak in the original phase's FFT result. In Fig. 2, the reference heart rate is 1.07 Hz according to the processing in Fig. 3, which means the true HR peak should be in the neighborhood of 1.07 Hz. In our system, we empirically define the neighborhood of the reference heart rate as $[ref - 0.1Hz, ref + 0.1Hz]$. Therefore, we will select the peak of 1.05 Hz as the true HR peak to proceed with the following steps rather than the peak of 0.79 Hz. In this way, TFiHR can help our system to deal with the problem of misleading frequency peaks in Fig. 2. Alg. 1 summarizes the steps of TFiHR.

5 Implementation and evaluation

In this section, we first introduce our system implementation, then explain our experimental setup and finally we evaluate the system and report our evaluation results. Specifically, we carefully evaluate factors that may impact our system's performance such as detecting distance, aiming point, depression angle, human orientation and beam width. Also, we study the performance with strong background interference. And finally, we evaluate our system in the more future realistic working environments.

5.1 System implementation

Hardware. We use *YunSDR Y310* as our baseband processing unit (BPU) to generate a baseband signal of 0.625MHz on the intermediate frequency (IF) carrier of 500MHz, and use a host to control and exchange the digital signal with the BPU over Ethernet. Then we use the 60 GHz front-ends *PEM009-KIT* to modulate and demodulate 60 GHz RF signal. The transmitter and receiver are synchronized by using the same reference clock. As for antennas, we use horn antennas with the gain of 20dBi, 24dBi and 34dBi. Figure 4 shows the structure of the mmWave platform.

Software. Our host runs signal processing algorithms written in C code, and can generate the estimation of respiratory rate and heart rate in real time. The FPGA of *YunSDR Y310* is programmed with the function of baseband processing using its native library. Figure 5 shows the data flow diagram of *MiVital*. Both the hardware and software can be transplanted into 60 GHz access points equipped with commercial phased array antennas.

5.2 Experimental setup

To imitate different beam patterns of phased array antennas by electronic beamforming, we apply directional antennas with different beam widths in this study. Since the work of human finding technique that helps the system to locate a user and the work of multi-user feasibility study has been accomplished in Yang et al. (2016), we focus on detecting the vital signs of a single user by varying the environmental factors and deploying in a more practical environment, and we suppose that our system can be extended to detect

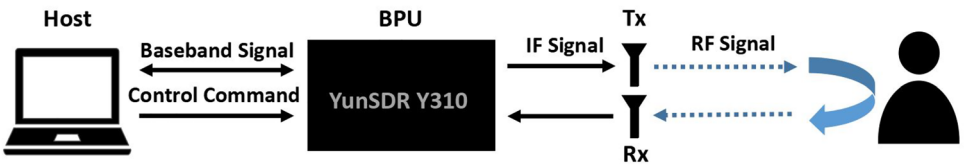

Fig. 4 MmWave Platform of *MiVital*. Our host can control and exchange baseband signals with the FPGA of BPU. The BPU can generate and process the intermediate frequency signal, and the 60 GHz front-ends (Tx and Rx) can transmit and receive mmWave signal

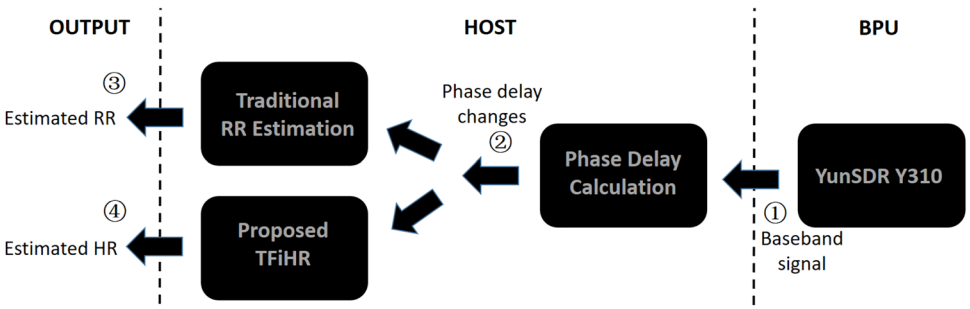

Fig. 5 Data flow diagram of *MiVital*. The host receives the reflected baseband signal from BPU and extracts phase delay changes. Then the host uses the phase delay changes to estimate RR and HR

vital signs of multi-user with the availability of phased array antennas and further transplanted into commercial 60 GHz access points.

Experiments. During the experiments, the user is required to sit on a chair facing the antennas and keep the body quasi-static. That is to say, he is allowed to move limbs or change sitting posture to relax sometimes. And the requirement of quasi-static is also mentioned in other state-of-the-art systems (Adib et al. 2015; Zhao et al. 2016). For each experiment, our system monitors the user for thirty seconds and applies signal processing algorithms to measure the RR and HR. To reduce the effect of random error, we repeat the above experimental procedure 10 times in each situation while fixing the position of user and antennas.

Participants. To evaluate the performance of our system, we enroll 12 participants (2 female) with the Body Mass Index (BMI) of $19-23kg/m^2$, age of $20-24$ years and weight of $54-72kg$. During the experiments, the user wore shirts, T-shirts, sweaters, and jackets with different fabric materials.

Ground truth. For respiratory rate, we count the number of complete breaths manually since the respiration movement is obvious and slow enough. As for heart rate, we use a medical-grade ECG (AD8232) device to acquire ECG waveform and then compute HR ground truth. For RR and HR of each experiment, we evaluate the accuracy of our system using the estimation error for breathing rate (Bpm) and heart rate (bpm).

Table 2 The range of four environmental factors in setup

Parameter	Range	Default value
Detecting distance	1, 2, ...7 m	1 m
Aiming position	Left chest, right chest, center, left abdominal, right abdominal	Center
Depression angle	0°, 20°, 40°, 60°	0°
Beam width	20°, 12°, 3°	3°
Human orientation	Front, back, left, right	Front

When considering the impact of each factor, we arrange the setup with default values

5.3 Performance comparison between Phase and RSS based detection

MmVital (Yang et al. 2016) use RSS of mmWave to monitor the vital sign of the user. However, RSS is insensitive to the minute chest movements caused by respiration and especially the more minute heartbeat. This is because the change of RSS is not only caused by the distance change between the human body and antennas but also seriously influenced by background and system noise. To support this idea, we record phase and RSS of reflected signal simultaneously and compare the performance of phase and RSS based detection in Fig. 6. From time domain in Fig. 6a, the large variations in phase change represent respiratory while the RSS changes are seriously influenced by noise. And from frequency domain in Fig. 6b, the peaks in red circles at 0.3 Hz and 1.1 Hz in the FFT result of phase respectively

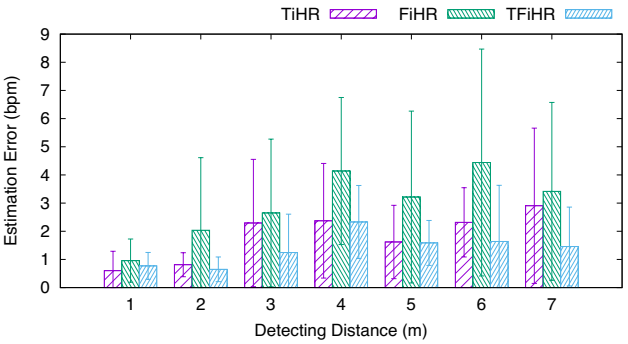

Fig. 7 Estimation error of three HR algorithms in different distances. TFiHR always performs the best in the three algorithms

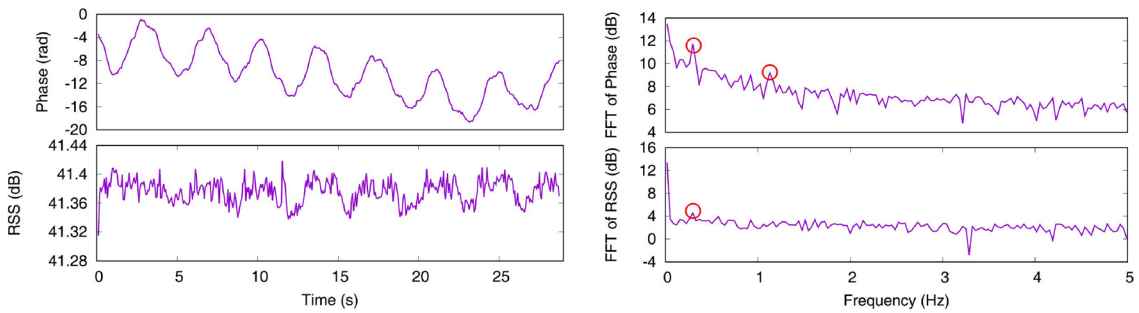

(a) Time domain

(b) Frequency domain

Fig. 6 **a** Changes of Phase and RSS in time domain. The large variations in Phase change represent respiratory while the RSS changes are seriously influenced by noise. **b** FFT results of Phase and RSS in frequency domain. In the FFT result of Phase, the peaks in red circles at 0.3 Hz and 1.1 Hz respectively represent RR and HR. But we can only find the RR peak at 0.3 Hz in the FFT result of RSS

represent RR and HR. But we can only find the RR peak at 0.3 Hz in the FFT result of RSS. Therefore, we'd like to use more insensitive phase for vital sign detection.

5.4 Performance of TFiHR compared with TiHR and FiHR

To evaluate the performance of TFiHR compared with the previous algorithms, we use the default setup in Table 2 and extend the detecting distance from 1 to 7 meters. For the received signal of each experiment, we apply three algorithms of FiHR, TiHR and TFiHR to get three estimations of HR. Figure 7 shows the heart rate estimation error of the three algorithms in different distances.

In the distance of less than 2 meters, all the three algorithms for heart rate detection perform well with the mean estimation error of less than 2 bpm. This is because the majority of the received signal within 2 meters is the effective reflected signal from user's body. As the distance gets larger, the estimation errors of three algorithms have an upward trend. With the larger detecting distance, the strength of effective reflected signal in the received signal is getting weaker. Then TiHR will be influenced by the sudden changes from background and phase noise, while FiHR will be seriously influenced by the periodic parts in the changes from background and phase noise. Thus both of their estimation error will increase gradually. However, by leveraging the global stability of TiHR and the local insensitivity of FiHR, TFiHR always performs the best and its estimation error keeps below 3 bpm.

5.5 Micro-Benchmark for HR detection

The practical scene is quite different from the previous simple scene and we'd like to analyze the difference from several micro-benchmark studies. Specifically, we will study the impact of environmental factors such as detecting distance, aiming position, human orientation and depression angle on the estimation error of HR. The experimental environment is an open space to reduce background noise. When considering the impact of one factor, we arrange the default setup in Table 2 first. We place the antennas together in front of the user for the distance of 1 meter, adjust the antennas at the same height as user's chest and adjust the antennas towards the center of user's front body. Then, we change the value of the target factor for different situations. In each situation, we use 3 types of antennas with different beam widths as listed in Table 2, and for each type of antenna, we repeat the experimental procedure 10 times.

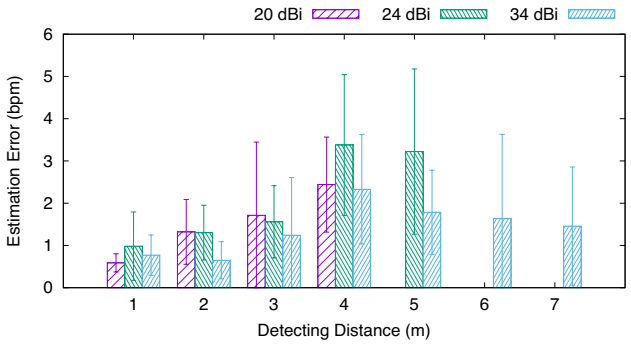

Fig. 8 Estimation error of HR when the antennas are in different distances from the user. The detecting distances of *MiVital* are 4*m*, 5*m* and 7*m* for 20, 24 and 34 dBi antennas

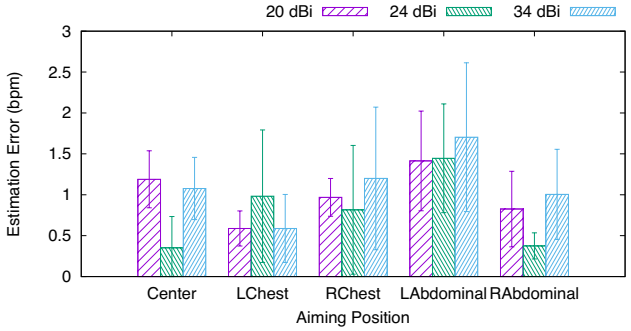

Fig. 9 Estimation error of HR when aiming at different positions of the human body. The "L" and "R" represent the left and right part of human body. *MiVital* is robust to detect HR when aiming at different point of human body

5.5.1 Accuracy of HR versus detecting distance

To verify that our system works well in its detection range, we ask the user to sit at different distances from the front-ends. As the distance becomes larger, the mmWave signal will get attenuated, and the coverage area of the signal will get larger which further weakens the effect of body movement caused by heartbeats. Figure 8 shows HR's estimation error of our experiments. When the user is out of *MiVital*'s detecting range, we can hardly detect the body movement and give up showing the estimation error in the figure. For distances of less than 2 meters, the estimation error can keep at 2 bpm using 20 dBi antenna. As distances get larger, the mean estimation error of HR will rise to 3 bpm but is still acceptable. And we can conclude that the detection range of 20 dBi antenna is about 4 meters. As for 24 dBi and 34 dBi antennas, the detection ranges are about 5 meters and 7 meters.

5.5.2 Accuracy of HR versus aiming position

Although the heart is always beating at the left chest of user's body, the effect of BCG is supposed not just limited to the left chest. Thus we'd like to study whether the position of the aiming point will impact the accuracy of HR. In Fig. 9, we plot the estimation error of HR when using all the three kinds of antennas and aiming at different positions (the center, left chest, right chest, left abdominal and right abdominal) of the human body. We can observe that the mean estimation error of HR is always less than 2 bpm when changing the factor of aiming point based on the default setup in Table 2. This shows that the effect of BCG is sufficient enough for our system to measure user's HR, as long as we are aiming at the front of the human body.

5.5.3 Accuracy of HR versus orientation

In the practical scene, the user will not always face the antennas, and it's necessary for us to study the performance when the user stays front, back, left and right to the antennas. The result in Fig. 10 shows that the human heartbeat can be detected from any orientations of the body. This shows that the BCG jitter caused by human heartbeat influences the whole body. From Fig. 10, we can also find that the mean estimation error of HR is less than 1.5 bpm when the user is front and back to the antennas. When the user is left or right to the antennas, the mean estimation error will increase but still keep under 3 bpm. This is because using the high directional mmWave horn antennas, the phase delay is sensitive to the body movement in the narrow antenna's beam. For front and back orientations, the mmWave signals are reflected by the flat chest and back of the body whose movements are mainly due to the vital signs of respiratory and heartbeat. However, for left and right orientations, the narrow beam can be easily blocked by the user's arms whose movements get little influence from human heartbeat and the periodic phase changes due to the heartbeat will get weak.

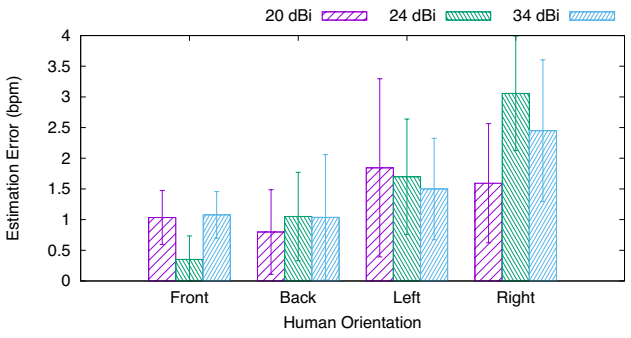

Fig. 10 Estimation error of HR with different human orientations. *MiVital* is robust to detect HR with different human orientations and it will be better for user to keep front or back to the antennas

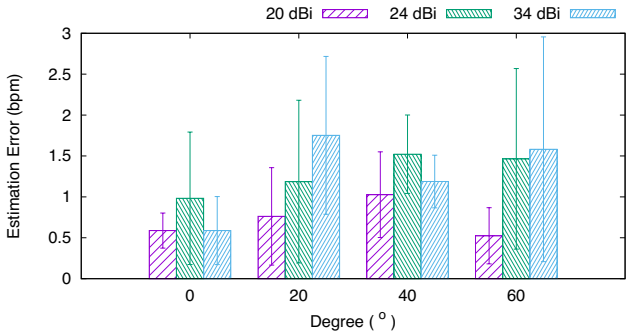

Fig. 11 Estimation error of HR with different depression angles. *MiVital* is robust to detect HR with different depression angles

5.5.4 Accuracy of HR versus depression angle

In the access point imitating experiment, the antennas are fixed on the ceiling, and the user may sit or rest at any place in the room. The depression angle of the antennas can get larger when the user stays under the antennas. Thus we'd like to discuss the impact of depression angle without changing detecting distance. Under the condition of the detecting distance of 1 meter, we move the antennas towards the user and raise the antennas properly to increase the depression angle. The result in Fig. 11 shows that the estimation error of HR is always less than 3 bpm. We can conclude that changing only the depression angle will not impact the accuracy of HR too much. Because the human body has an irregular surface rather than a flat "mirror", the receiver can still capture the reflected signal even with a large depression angle of 60 degrees. Moreover, the received signal is still strong enough to detect the human body movement with this large depression angle.

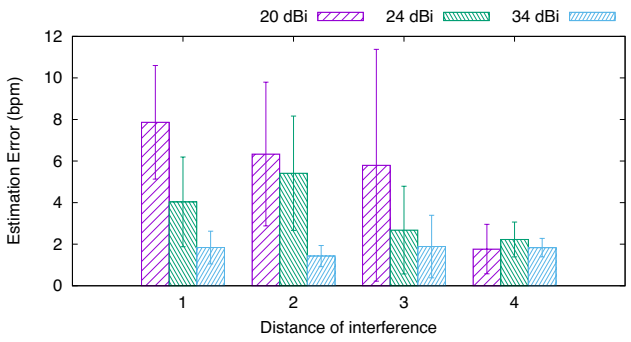

Fig. 12 Estimation error of HR when the interference person is walking around behind the user in different distances

5.6 Performance of HR detection with strong background interference

Having proved that our system is robust with tiny changes from the background, we consider the strong background interference such as moving objects or human body behind the user in the practical scene. To control the background interference in different levels, we conduct the experiments by putting the antennas at a distance of $3m$ from the user and ask another participant to walk around behind the user at different distances from $1m$ to $4m$. We study the performance on different beam widths and show the estimation error in Fig. 12.

The HR detection using 20 dBi antennas is seriously influenced when the interference person is within the distance of $3m$ from the user. The interference-free distance is $4m$ where the mean estimation error is lower than 3 bpm. As for 24 dBi and 34 dBi antennas, the interference-free distances are $3m$ and $1m$, respectively. We can see that when the interference person is sufficiently far from the user, it will not interfere with HR detection. And the interference-free distance is shorter for antennas with narrower beam width because of less background noise.

5.7 Performance of access point imitating experiments

Finally, we'd like to evaluate the system performance in a practical working environment by imitating an access point mounted on the ceiling. In the future, we envision that the vital sign detection system runs on an 802.11ad router and the access points hang on the ceiling or are fixed on the wall. Both devices transmit and receive mmWave signals. Therefore, we deploy our system by mounting a mmWave access point on the ceiling and conduct our experiments in two scenes: an open space and a cluttered office room.

5.7.1 Access point imitating in an open space

The first scene is an open space as shown in Fig. 13a. During the experiments, we place the directional transmitting and receiving antennas at the coordinate of (−0.5, 1.5) and (−0.5, 2.5) in Fig. 13b with a height of 2.5 meters. For each experiment, we first refer to the human finding algorithm developed in Yang et al. (2016) and manually adjust the direction of antennas towards the user according to the phase variation. After that, the system starts to detect user's vital sign. For each of the 24 squares, we randomly select two of

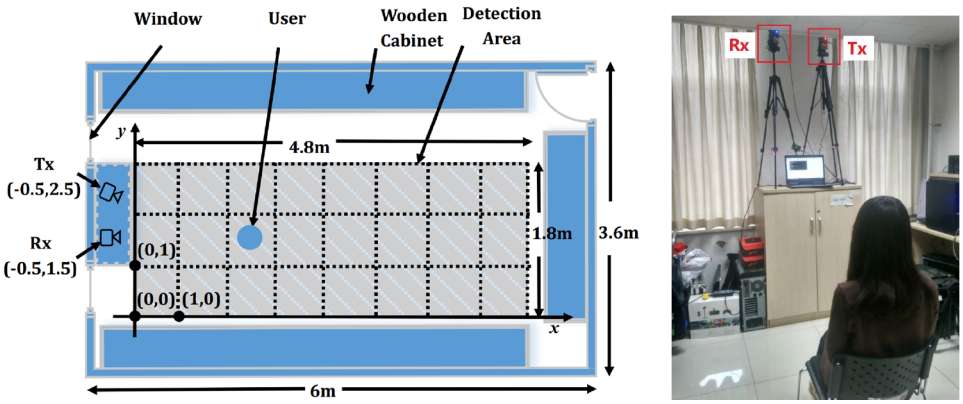

(a) Environment layout (b) Experimental setup

Fig. 13 **a** The experimental environment of an open space in an office room. The detection area is divided into 8×3 squares. **b** The set up of mmWave device where the antennas are set near the ceiling

(a) 20 dBi antenna (b) 24 dBi antenna (c) 34 dBi antenna

Fig. 14 Estimation error of HR using different antennas in the access point imitating experiments. The square at the coordinate of (2.5, 1.5) has the most robust accuracy of HR to different antennas

the participants and conduct experiments using the 3 types of antennas with different beam widths. In the following subsections, we'll analyze the accuracy of HR and RR in the access point imitating experiments.

Accuracy of HR. The black parts in Fig. 14 represent that our system can hardly detect the vital sign of user sitting in these places. The result shows that with 20dBi antennas, our system can detect the vital sign of user within 3 meters. With 24 dBi antennas, our system can detect the vital sign of user within about 4.2 meters, while the 34 dBi antennas can expand detection range to cover the whole detection area in Fig. 13a. It's obvious that when the beam width of antennas is narrower, the detection range is larger.

In the working range for each antenna, the HR estimation error of our system is always less than 6 bpm. Besides, for the same place, the estimation error will often get lower using antennas with narrower beam width. Combining the result of three kinds of antennas, we can also conclude that the square at the coordinate of (2.5, 1.5) has the most robust accuracy of heart rate. When the user sits at this place, the height of his chest is about 1 meter and then the relative height of antennas to user's chest is about 1.5 meters. Then the detecting distance is about 2.3 meters and the depression angle is about 40°. Both of them are in the appropriate range of our system.

Finally, our system is always robust and accurate when the user is in its detection range, and the overall estimation error of HR in this access point imitating experiment can keep at 2.386 bpm by averaging the estimation errors of experiments in all the squares. The HR accuracy of our system is comparable to that of MmVital (Yang et al. 2016) whose mean estimation error of HR is 2.15 bpm but our experiments are conducted in a more practical scene.

Accuracy of RR. As shown in Fig. 15, the measurement result of RR is always accurate (less than 1 Bpm estimation error) in the working range. Besides, the difference between the estimated respiratory cycles by our system and the ground truth is always within one cycle. By averaging the accuracies of experiments in all the squares, the overall estimation error of RR can keep at 0.487 Bpm in the open space which is also comparable to MmVital Yang et al. (2016)'s RR mean estimation error of 0.43 Bpm.

5.7.2 Access point imitating in a cluttered office room

After evaluating the accuracy of HR and RR in the open space, we'd like to further verify the robustness of our system in a cluttered office room as shown in Fig. 16a. The room is full of wooden desks, PCs and other devices. These objects will introduce many multipath reflections and further

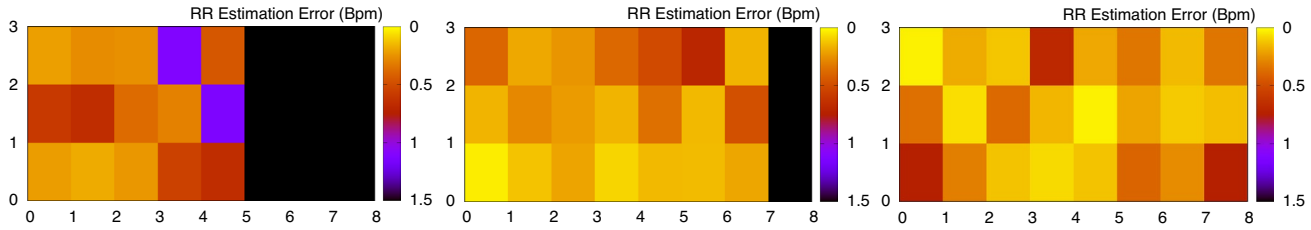

(a) 20 dBi antenna (b) 24 dBi antenna (c) 34 dBi antenna

Fig. 15 Accuracy of RR using different antennas in the access point imitating experiments. *MiVital* is robust to estimate user's RR in its working range

Fig. 16 **a** The experimental environment of a typical cluttered office room. **b** The set up of mmWave device where the antennas are set near the ceiling

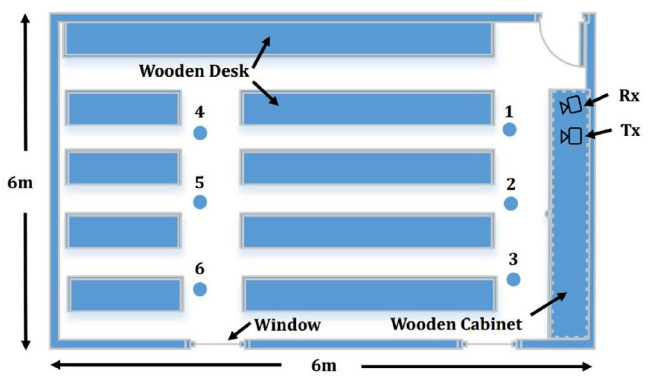

(a) Environment layout

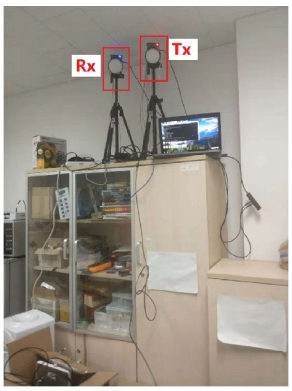

(b) Experimental setup

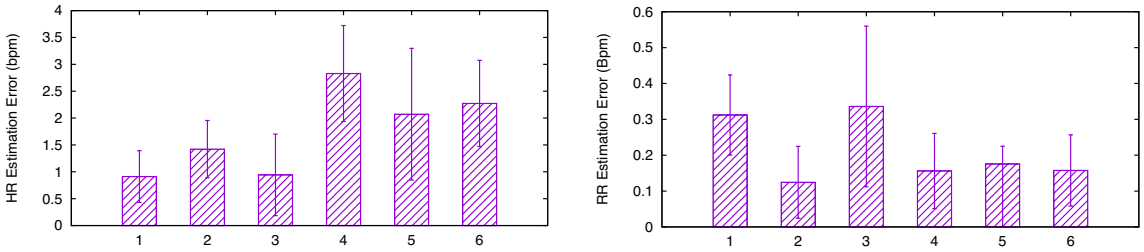

(a) HR estimation error (b) RR estimation error

Fig. 17 Estimation errors of HR (**a**) and RR (**b**) in the cluttered office room for user in six points. User at point 1, 2 and 3 has the best HR accuracy

influence the detecting accuracy when we detect user's vital sign. To evaluate our system's performance, We place the directional transmitting and receiving antennas on a wooden cabinet under the ceiling in Fig. 16b with a height of 2.5 m. For each experiment, we follow the same experimental procedure in Sect. 5.7.1. For each test point, we randomly select three of the participants and conduct experiments 10 times using the 34 dBi antennas because only the 34 dBi antennas have a large enough detecting range to cover the whole room.

The result in Fig. 17a shows that for the points close to the antennas (1, 2 and 3), the estimation error of HR is quite low (less than 1.5 bpm) while for those far from the antennas (4, 5 and 6), the estimation error of HR will increase to $2 \sim 3$ bpm. Although the system can detect user's heartbeat at all points, long-distance heart rate detection will still be influenced by the reflection of surrounding objects. As for RR detection shown in Fig. 17b, the system has an accurate RR estimation in all six points with a mean estimation error of less than 0.4 Bpm. This is because the chest movement caused by respiratory is large enough for a narrow beam to accurately detect.

After comparing the experimental results in the open space environment and the cluttered environment, we can conclude that the accuracy of HR estimation will be influenced by the objects near the users because of multipath reflections. This phenomenon is more obvious in a cluttered environment especially when the user is far from the antennas with large background noise.

6 Limitations and Discussion

The influence of sidelobes. The sidelobe effect can't be ignored in the beam pattern of the phased array antennas. However, the gain of sidelobe is much lower than that of mainlobe. Besides, when the main lobe is aiming at the user in the line of sight, the beam arriving at side lobe will experience more attenuation because of longer transmission distance. Therefore, we believe the influence of sidelobes is little in the line of sight situation for a single user.

Random body motion cancellation. RBM cancellation is a significant challenge to be handled. Our system works when the user is sitting still and suffers from RBM. Here, we provide a possible solution: with two transmitters aiming at different positions of the user's body, we may be able to detect the vital sign by comparing the two received signals when the user is under one-dimensional random body motion. We leave this solution for future work.

Recent 60 GHz mmWave phased array antennas. Nowadays, 60 GHz mmWave phased array antennas have been used widely for electronic beam-steering in research (Wang et al. 2020; Zhao et al. 2020; Zhang et al. 2016; Saha et al. 2019; Lacruz et al. 2020). Among the available 60 GHz phased array antennas, the commodity 802.11ad radio from Airfide Inc. Airfide Networks (2019) used in Wang et al. (2020); Zhao et al. (2020) applies the maximum number of antenna elements (6×6 elements). However, the beam patterns generated by these 60 GHz phased arrays cannot satisfy the needs of room-level vital sign detection due to the limited number of antenna elements and discrete beamforming weight control. Specifically, the current phased array antennas face the following situations compared to the horn antennas we use. First, the gains of their beam patterns are much smaller than the gains of directional horn antennas, but the path loss is quite large for vital sign detection after the 60 GHz signal is reflected by human body. Second, current 60 GHz phased array antennas have much larger beam widths than directional horn antennas and introduce stronger background interference. Third, the sidelobe suppression performance for current 60 GHz phased array antennas are not as good as directional horn antennas, and the sidelobes can also introduce more background interference. Therefore, we believe that the performances of horn antennas are more similar to those of the future 60 GHz phased array antennas with much more antenna elements.

7 Conclusion

In this article, we verify the feasibility of mmWave vital sign detection in practical scenes by implementing a phase-modulated system on the software-defined radio platform. Also, we develop a time-domain and frequency-domain information based HR detection algorithm for heart rate detection by leveraging the global stability of TiHR and the local insensitivity of FiHR. We verify its robustness by studying the impact of multiple environmental factors and deploying our system on the ceiling to imitate an access point. The results show that the system can provide accurate and robust RR and HR estimations, which is comparable with state-of-the-art mm Wave systems, and work at a further distance of up to 7 meters. Our system can be transplanted into future 60 GHz phased array antennas with larger antenna elements and narrower beams.

References

Abdelnasser, H., Harras, K.A., Youssef, M.: Ubibreathe: A ubiquitous non-invasive wifi-based breathing estimator. ACM MobiHoc (2015)

Adib, Fadel, Mao, Hongzi, Kabelac, Zachary, Katabi, Dina, Miller, Robert C.: Smart homes that monitor breathing and heart rate. ACM CHI (2015)

Airfide Networks. Airfide-A 5G Company (2019). http://airfidenet.com

Anttonen, Jenni, Surakka, Veikko: Emotions and heart rate while sitting on a chair. In: Proceedings of the SIGCHI conference on Human factors in computing systems, pp. 491–499. ACM (2005)

Bianchi, A.M., Mendez, M.O., Cerutti, S.: Processing of signals recorded through smart devices: sleep-quality assessment. IEEE Trans. Inf Technol. Biomed. **14**(3), 741–747 (2010)

Bonde, Amelie, Pan, Shijia, Jia, Zhenhua, Zhang, Yanyong, Noh, Hae Young, Zhang, Pei: Vvrrm: Vehicular vibration-based heart rr-interval monitoring system. In: Proceedings of the 19th International Workshop on Mobile Computing Systems & Applications, pp. 37–42. ACM (2018)

Bruser, C., Stadlthanner, K., de Waele, S., Leonhardt, S.: Adaptive beat-to-beat heart rate estimation in ballistocardiograms. IEEE Trans. Inf Technol. Biomed. **15**(5), 778–786 (2011)

Chen, Baicheng, Li, Huining, Li, Zhengxiong, Chen, Xingyu, Xu, Chenhan, Xu, Wenyao: Thermowave: a new paradigm of wireless passive temperature monitoring via mmwave sensing. In: Proceedings of the 26th Annual International Conference on Mobile Computing and Networking, pp. 1–14 (2020)

Chenshu, W., Zhang, F., Wang, B., Liu, K.J.R.: msense: Towards mobile material sensing with a single millimeter-wave radio. Proc. ACM Interact. Mobile Wearable Ubiquitous Technol. **4**(3), 1–20 (2020)

Chuang, H.-R., Kuo, H.-C., Lin, F.-L., Huang, T.-H., Kuo, C.-S., Ou, Y.-W.: 60-ghz millimeter-wave life detection system (mlds) for noncontact human vital-signal monitoring. Sensors J. IEEE (2012)

Chung, Gih Sung, Choi, Byoung Hoon, Jeong, Do-Un, Park, Kwang Suk: Noninvasive heart rate variability analysis using loadcell-installed bed during sleep. In: Engineering in Medicine and Biology Society, 2007. EMBS 2007. In: 29th Annual International Conference of the IEEE, pp. 2357–2360. IEEE (2007)

Eduardo, P., Octavian, P., Pedro, G.: Theory and developments in an unobtrusive cardiovascular system representation: Ballistocardiography. Open Biomed. Eng. J. **4**(1), 201 (2010)

Grenvik, A., Ballou, S., McGinley, E., Millen, J.E., Cooley, W.L., Safar, P.: Impedance pneumography: comparison between chest impedance changes and respiratory volumes in 11 healthy volunteers. Chest **62**(4), 439–443 (1972)

Griffiths, Erin, Saponas, T. Scott, Brush, A.J.: Health chair: implicitly sensing heart and respiratory rate. In: Proceedings of the 2014 ACM International Joint Conference on Pervasive and Ubiquitous Computing, pp. 661–671. ACM (2014)

Høst-Madsen, Anders, Petrochilos, Nicolas, Boric-Lubecke, Olga, Lubecke, Victor M., Park, Byung-Kwon, Zhou, Qin: Signal processing methods for doppler radar heart rate monitoring. In: Signal processing techniques for knowledge extraction and information fusion, pp. 121–140. Springer (2008)

Jason Kao, Te-Yu, Lin, Jenshan: Vital sign detection using 60-ghz doppler radar system. Wireless Symposium (IWS) (2013)

Jia, Zhenhua, Alaziz, Musaab, Chi, Xiang, Howard, Richard E., Zhang, Yanyong, Zhang, Pei, Trappe, Wade, Sivasubramaniam, Anand, An, Ning: Hb-phone: a bed-mounted geophone-based heartbeat monitoring system. In: Information Processing in Sensor Networks (IPSN), 2016 15th ACM/IEEE International Conference on, pp. 1–12. IEEE (2016)

Jia, Zhenhua, Bonde, Amelie, Li, Sugang, Xu, Chenren, Wang, Jingxian, Zhang, Yanyong, Howard, Richard E., Zhang, Pei: Monitoring a person's heart rate and respiratory rate on a shared bed using geophones. In: Proceedings of the 15th ACM Conference on Embedded Network Sensor Systems. ACM (2017)

Jiang, Chengkun, Guo, Junchen, He, Yuan, Jin, Meng, Li, Shuai, Liu, Yunhao: mmvib: micrometer-level vibration measurement with mmwave radar. In: Proceedings of the 26th Annual International Conference on Mobile Computing and Networking, pp. 1–13 (2020)

Kortelainen, J.M., van Gils, M., Parkka, J.: Multichannel bed pressure sensor for sleep monitoring. Comput. Cardiol. **39**, 313–316 (2012)

Lacruz, Jesus Omar, Garcia, Dolores, Mateo, Pablo Jiménez, Palacios, Joan, Widmer, Joerg: mm-flex: an open platform for millimeter-wave mobile full-bandwidth experimentation. In: Proceedings of the 18th International Conference on Mobile Systems, Applications, and Services, pp. 1–13 (2020)

Li, Xiaobai, Chen, Jie, Zhao, Guoying, Pietikäinen, Matti: Remote heart rate measurement from face videos under realistic situations 4264–4271 (2014)

Li, C., Lin, J.: Random body movement cancellation in doppler radar vital sign detection. IEEE Trans. Microw. Theory Tech. **56**(12), 3143–3152 (2008)

Lin, Feng, Song, Chen, Zhuang, Yan, Xu, Wenyao, Li, Changzhi, Ren, Kui: Cardiac scan: A non-contact and continuous heart-based user authentication system. In: The International Conference, pp. 315–328 (2017)

Liu, Jian, Wang, Yan, Chen, Yingying, Yang, Jie, Chen, Xu, Cheng, Jerry: Tracking vital signs during sleep leveraging off-the-shelf wifi. ACM MobiHoc (2015)

Mayo Clinic What's a normal resting heart rate? (2018). http://www.mayoclinic.org/healthy-living/fitness/expert-answers/heart-rate/faq-20057979. Accessed 1 Nov 2018

Nguyen, Phuc, Zhang, Xinyu, Halbower, Ann, Vu, Tam: Continuous and fine-grained breathing volume monitoring from afar using wireless signals. In: IEEE INFOCOM 2016 - the IEEE International Conference on Computer Communications, pp. 1–9 (2016)

Phan, D.H., Bonnet, S., Guillemaud, R., Castelli, E., Pham Thi, N.Y.: Estimation of respiratory waveform and heart rate using an accelerometer. In: Engineering in Medicine and Biology Society, 2008.

EMBS 2008. 30th Annual International Conference of the IEEE, pp. 4916–4919. IEEE (2008)
Ravichandran, Ruth, Saba1, Elliot, Chen, Ke-Yu, Goel, Mayank, Gupta, Sidhant, Patel, Shwetak N.: Wibreathe: Estimating respiration rate using wireless signals in natural settings in the home. IEEE PerCom (2015)
Rosales, Licet, Skubic, Marjorie, Heise, David, Devaney, Michael J., Schaumburg, Mark: Heartbeat detection from a hydraulic bed sensor using a clustering approach. In: Engineering in Medicine and Biology Society (EMBC), 2012 Annual International Conference of the IEEE, pp. 2383–2387. IEEE (2012)
Saha, S.K., Ghasempour, Y., Haider, M.K., Siddiqui, T., De Melo, P., Somanchi, N., Zakrajsek, L., Singh, A., Shyamsunder, R., Torres, O., et al.: X60: A programmable testbed for wideband 60 ghz wlans with phased arrays. Comput. Commun. **133**, 77–88 (2019)
Santhalingam, P.S., Hosain, A.A., Zhang, D., Pathak, P., Rangwala, H., Kushalnagar, R.: mmasl: Environment-independent asl gesture recognition using 60 ghz millimeter-wave signals. Proc. ACM Interact. Mobile Wearable Ubiquitous Technol. **4**(1), 1–30 (2020)
Šprager, S., Zazula, D.: Detection of heartbeat and respiration from optical interferometric signal by using wavelet transform. Comput. Methods Programs Biomed. **111**(1), 41–51 (2013)
Sun, Feng-Tso, Kuo, Cynthia, Cheng, Heng-Tze, Buthpitiya, Senaka, Collins, Patricia, Griss, Martin: Activity-aware mental stress detection using physiological sensors. In: International Conference on Mobile Computing, Applications, and Services, pp. 282–301. Springer (2010)
U.S. National Library of Medicine. Rapid Shallow Breathing (2018). https://medlineplus.gov/ency/article/007198.htm. Accessed 1 Nov 2018
Tse, D., Pramod, V.: Fundamentals of wireless communications. Cambridge University Press, Cambridge (2005)
Wang, Hao, Zhang, Daqing, Ma, Junyi, Wang, Yasha, Wang, Yuxiang, Wu, Dan, Gu, Tao, Xie, Bing: Human respiration detection with commodity wifi devices: Do user location and body orientation matter? ACM UbiComp (2016)
Wang, Song, Huang, Jingqi, Zhang, Xinyu, Kim, Hyoil, Dey, Sujit: X-array: Approximating omnidirectional millimeter-wave coverage using an array of phased arrays. In: Proceedings of the 26th Annual International Conference on Mobile Computing and Networking, pp. 1–14 (2020)
Wang, Xuyu, Yang, Chao, Mao, Shiwen: Phasebeat: Exploiting csi phase data for vital sign monitoring with commodity wifi devices. In: Distributed Computing Systems (ICDCS), 2017 IEEE 37th International Conference on, pp. 1230–1239. IEEE (2017)
Wang, X., Yang, C., Mao, S.: Tensorbeat: Tensor decomposition for monitoring multiperson breathing beats with commodity wifi. ACM Trans. Intell. Syst. Technol. (TIST) **9**(1), 8 (2017)
Wei, Teng, Zhang, Xinyu: mtrack: High-precision passive tracking using millimeterwave radios. ACM MobiCom (2015)
Wu, Chenshu, Zhang, Feng, Wang, Beibei, Liu, K.J. Ray: mmtrack: Passive multi-person localization using commodity millimeter wave radio. In: IEEE INFOCOM 2020-IEEE Conference on Computer Communications, pp. 2400–2409. IEEE (2020)
Wu, Ting, Rappaport, Theodore S., Collins, Christopher M.: The human body and millimeter-wave wireless communication systems: Interactions and implications **27**(1), 2423–2429 (2015)
Yang, Zhicheng, Pathak, Parth H., Zeng, Yunze, Liran, Xixi, Mohapatra, Prasant: Monitoring vital signs using millimeterwave. ACM MobiHoc (2016)
Zeng, Y., Dan, W., Gao, R., Tao, G., Zhang, D.: Fullbreathe: Full human respiration detection exploiting complementarity of csi phase and amplitude of wifi signals. Proc. ACM Interact. Mobile Wearable Ubiquitous Technol. **2**(3), 148 (2018)
Zeng, Y., Wu, D., Xiong, J., Yi, E., Gao, R., Zhang, D.: FarSense. Pro. ACM Interact. Mobile, Wearable Ubiquitous Technol. **3**(3), 1–26 (2019). https://doi.org/10.1145/3351279
Zhang, Jialiang, Zhang, Xinyu, Kulkarni, Pushkar, Ramanathan, Parameswaran: Openmili: A 60 ghz software radio platform with a reconfigurable phased-array antenna. In: Proceedings of the 22nd Annual International Conference on Mobile Computing and Networking, pp. 162–175 (2016)
Zhao, Mingmin, Adib, Fadel, Katabi, Dina: Emotion recognition using wireless signals. ACM MobiCom (2016)
Zhao, Renjie, Woodford, Timothy, Wei, Teng, Qian, Kun, Zhang, Xinyu: M-cube: A millimeter-wave massive mimo software radio. In: Proceedings of the 26th Annual International Conference on Mobile Computing and Networking, pp. 1–14 (2020)
Zimetbaum, P.J., Josephson, M.E.: The evolving role of ambulatory arrhythmia monitoring in general clinical practice. Ann. Intern. Med. **130**(10), 848–56 (1999)

Weicheng Wang received the B.S. degree in Computer Science from Peking University in 2017. He is currently working toward the M.S. degree at Center for Energy-efficient Computing and Applications in Peking University, China. His research interests include wireless sensing and mobile computing.

Zhenhua Jia received his Ph.D. degree in Computer Engineering from the Department of Electrical and Computer Engineering, Rutgers University-New Brunswick in 2019. He is currently a senior R&D engineer at NVIDIA focusing on perception models for Autonomous Driving. His research interests include Ubiquitous Computing, Cyber Physical Systems, and Autonomous Driving.

Chenren Xu is a Boya Young Fellow Assosiate Professor (with early tenure) in the School of Computer Science at Peking University (PKU) where he directs Software-hardware Orchestrated ARchitecture (SOAR) Lab. His research interests span wireless, networking and system, with a current focus on backscatter communication for low power IoT connectivity, future mobile Internet for high mobility data networking, and collaborative edge intelligence system for mobile and IoT computing. He earned his Ph.D. from WINLAB, Rutgers University, and worked as postdoctoral fellow in Carnegie Mellon University and visiting scholars in AT&T Shannon Labs and Microsoft Research. He is the Associate Editors of ACM IMWUT and Communications of the CCF. He published papers and has been serving as organization commitee and/or TPC in top venues including ACM SIGCOMM, MobiCom, SenSys, UbiComp and IEEE INFOCOM. He is a recipient of NSFC Excellent Young Scientists Fund (2020), Alibaba DAMO Academy Young Fellow (2018), ACM SIGCOMM China Rising Star (2020), CCF-Intel Young Faculty (2017) and CIE Outstanding Scientific and Technological Worker (2021) awards. His work has been featured in MIT Technology Review.

Guojie Luo received the B.S. degree in computer science from Peking University, Beijing, China, in 2005 and the M.S. and Ph.D. degrees in computer science from the University of California at Los Angeles, Los Angeles, CA, USA, in 2008 and 2011, respectively. He is currently an Associate Professor at the Center for Energy-efficient Computing and Applications (CECA) with the School of Computer Science, Peking University. Dr. Luo was a recipient of the 2013 ACM SIGDA Outstanding Ph.D. Dissertation Award in Electronic Design Automation and the 10 year Retrospective Most Influential Paper Award with ASPDAC 2017. His research interests include design automation for emerging computer architectures.

Daqing Zhang (Fellow, IEEE) is with the Key Laboratory of High Confidence Software Technologies, School of Computer Science, Peking University, Beijing, China, and Telecom SudParis, France. His research interests include context-aware computing, urban computing, mobile computing, big data analytics, pervasive elderly care, etc. He received his Ph.D. degree from the University of Rome "La Sapienza" Rome, Italy, in 1996. He is the Associate Editor for IEEE Pervasive Computing, ACM Transactions on Intelligent Systems and Technology, and the Proceeding of ACM on Interactive, Mobile, Wearable and Ubiquitous Technologies. He is the winner of the Ten-Years Impact Paper Award at IEEE PerCom 2013 and IEEE UIC 2019, the Honorable Mention Award at ACM UbiComp 2015 and 2016, the Distinguished Paper Award at ACM UbiComp 2021, the Best Paper Award at IEEE UIC 2015 and 2012.

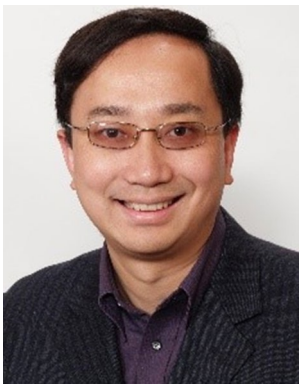

Ning An has a Ph. D. in Computer Science and Engineering from the Pennsylvania State University, USA. He is a Fellow of the International Academy of Health Sciences Informatics (FIAHSI) and an IEEE Senior Member. In 2011, Dr. An joined the Hefei University of Technology as a "Yellow Mountain" Distinguished Professor and founded the HFUT Gerontechnology Lab, the first in mainland China. It was accredited in 2016 by the Ministry of Science and Technology (MOST) of the People's Republic of China as the National International Collaboration Base for Smart Eldercare. Before HFUT, Dr. An had worked at Oracle Inc. in the United States as a technical staff member for ten years. His research interests include Social Technology, Data Science and Engineering, and Health Informatics. In addition to publishing more than seventy peerreviewed papers in international journals and international conferences, Dr. An published two books, two book chapters and wrote four granted US patents and eighteen Chinese granted patents.

Yanyong Zhang received her B.S. from the University of Science and Technology of China (USTC) in 1997, and Ph.D. from Penn State University in 2002. From 2002 and 2018, she was on the faculty of the Electrical and Computer Engineering Department at Rutgers University. She was also a member of the Wireless Information Networks Laboratory (Winlab). Since July 2018, she joined the school of Computer Science and Technology at USTC. She has 21 years of research experience in the areas of sensor networks, ubiquitous computing, and high-performance computing, and has published more than 140 technical papers in these fields. She received the NSF CAREER award in 2006, and was elevated to IEEE Fellow in 2017. She has served/currently serves as the Associate Editor for several journals, including IEEE/ACM Transactions on Networking, IEEE Transactions on Mobile Computing, IEEE Transactions on Service Computing, IEEE Transactions on Dependable and Secure Computing, and Elsevier Smart Health. She has served on various conference TPCs including DSN, Sensys, Infocom, etc. She is the TPC co-chair for IPSN'22.